UNIVERSITY OF CALIFORNIA,
IRVINE

Predicting Droplet Formation on Centrifugal Microfluidic Platforms

THESIS

Submitted in partial satisfaction of the requirements
for the degree of

MASTER OF SCIENCE

in Biomedical Engineering

by

Jacob Alfred Moebius

Thesis Committee:
Professor Marc Madou, Chair
Professor Abraham Lee
Professor William Tang

2015

DEDICATION

To

My mother Kim and brother Aaron for their constant love and support throughout all of the ups and downs. Their sacrifices allowed me to pursue my dreams and aspirations.

Staci Galvin-Castro for her love and support over the years, for bringing out the best in me, and for the inspiration she gives me to never stop shooting for the stars.

Ms. (Dr.) Marietta Dunaway and the Campolindo High School Science Department for inspiring me to pursue the sciences. Without their teaching, I never would have come as far as I have today.
R.I.P. Ms. Dunaway.

TABLE OF CONTENTS

LIST OF FIGURES

LIST OF TABLES

ACKNOWLEDGEMENTS

I would like to thank Dr. Marc Madou for his support not only during graduate school, but also during my undergraduate career. I am thankful for him giving me the many opportunities that would have been out of my reach otherwise. He helped me break past the limits that I thought I had, and made me a better researcher and engineer.

I would like to thank my committee members Dr. Abraham Lee and Dr. William Tang for their direction and insight for this work. I sincerely appreciate the thoughtful feedback for this project provided by Dr. Lee. I am grateful for the guidance that Dr. Tang has provided me since I was an undergraduate. The work that he does for us students is truly inspirational.

I would like to thank Dr. Lawrence Kulinsky, Dr. Horacio Kido, and Dr. Regis Peytavi, along with the students of the UCI BioMEMS group. The mentorship, insight, and camaraderie that they all provided made me a better engineer. For that, I am grateful.

I would like to thank Dr. Mindy Simon for guiding me on this journey. Her knowledge, patience, and direction regarding this work were outstanding. I could not have asked for a better colleague, and I know many others share the same appreciation.

I would like to thank my undergraduates Patrick Manalo, Melinda Preedanon, and Justin Stovner for their hard work both on this project and the ones that follow. They are one of the most significant reasons why I worked so hard to get this far.

Financial support provided by the Advanced Manufacturing Partnership Grant.

ABSTRACT OF THE THESIS

Predicting Droplet Formation

on Centrifugal Microfluidic Platforms

By

Jacob Alfred Moebius

Master of Science in Biomedical Engineering

University of California, Irvine, 2015

Professor Marc Madou, Chair

Centrifugal microfluidics is a widely known research tool for biological sample and water quality analysis. Currently, the standard equipment used for such diagnostic applications include slow, bulky machines controlled by multiple operators. These machines can be condensed into a smaller, faster benchtop sample-to-answer system.

Sample processing is an important step taken to extract, isolate, and convert biological factors, such as nucleic acids or proteins, from a raw sample to an analyzable solution. Volume definition is one such step. The focus of this thesis is the development of a model predicting

monodispersed droplet formation and the application of droplets as a technique for volume definition.

First, a background of droplet microfluidic platforms is presented, along with current biological analysis technologies and the advantages of integrating such technologies onto microfluidic platforms. Second, background and theories of centrifugal microfluidics is given, followed by theories relevant to droplet emulsions. Third, fabrication techniques for centrifugal microfluidic designs are discussed. Finally, the development of a model for predicting droplet formation on the centrifugal microfluidic platform are presented for the rest of the thesis.

Predicting droplet formation analytically based on the volumetric flow rates of the continuous and dispersed phases, the ratios of these two flow rates, and the interfacial tension between the continuous and dispersed phases presented many challenges, which will be discussed in this work. Experimental validation was completed using continuous phase solutions of different interfacial tensions. To conclude, prospective applications are discussed with expected challenges.

CHAPTER 1: Introduction to Droplet and Centrifugal Microfluidics

1.1 Introduction to Droplet Microfluidics

Droplet generation is a useful analytical tool in microfluidics. Each droplet contains a volume of an aqueous sample, ranging from microliters to attoliters, and is used as a micro reaction chamber.[1,2] Droplet emulsions consists of an aqueous dispersed phase that contains a target analyte and an inorganic continuous phase that separates and carries minute volumes of the analyte solution. Utilizing the small size of droplets, the diffusion length to mix and heat solutions is reduced, shortening reaction time and heat transfer duration, tests can easily be multiplexed, sample volume is decreased, and a high throughput is achieved for volume definition and analysis.[3–5] Due to these traits, droplet microfluidics is an enticing method to carry out polymerase chain reaction (PCR) protocols,[6–8] drug delivery,[9] cell encapsulation,[10–12] pharmaceutical studies,[13] and bioreactor and chemical reactor experiments.[14,15]

While typically performed on Lab-on-Chip (LoC) devices with external syringe pumps, droplet microfluidics and its integration onto centrifugal microfluidic devices – specifically the Lab-on-Disk (LoD) platform – are explored in this work. Syringe pumps are an effective method to control the amount of pressure used to drive fluid flow on LoC platforms. LoD devices, however, use a motor to not only pump fluids, but to also process and multiplex samples.[16] As appealing as a closed micro total analysis system (μTAS) is, it is difficult to integrate the advantages of droplet microfluidics onto LoD platforms due to the lack of understanding of the physics of droplet generation on LoD systems. One specific difficulty is the uniformity of the pumping accomplished by the motor. Rather than tuning the forces of each individual chamber to pump at different pressures, the motor produces a uniform force around the same radius of the

entire fluidic disk. So, dispersed phase and continuous phase solutions of different densities call for an adjustment to the radial position of each liquid prior to the production of each fluidic disk. Also, the fluid level in the chambers are not constant, and the flow rates of the dispersed phase and continuous phase are different. Interfacial tension between the two phases is another contributing factor to the difficulty of integrating droplet production onto LoD platforms. This work discusses the investigation into these difficulties.

1.2 Centrifugal Microfluidics Fundamentals

Centrifugal microfluidics originated in the late 1960s with Anderson's research of a centrifugal analyzer.[17] Since then, the desire for an automated bedside sample-to-answer devices has grown due to the increasing number of different diagnostic tests and the high technical skill required to execute these tests. Microfluidic platforms are a possible answer to this growing demand. When compared to current diagnostic technologies, both LoC and LoD devices use reduced sample volumes and are capable of performing complex diagnostic tests with fluid manipulation mechanisms such as valving, metering, mixing, etc. Also, both platforms complete tests in shorter amounts of time and are mass producible via molding techniques.[18] As previously stated, the LoD platform uses a motor as a pump. Rotational pseudo-forces, such as centrifugal, Coriolis, and Euler, generated by the motor are independent of certain physiological properties, such as pH or ionic strength, providing an advantage over electroosmotic pumping.[19] These pseudo-forces can also drive raw sample preparation and processing. Examples of sample preparation and processing include mechanical lysing,[20] separating particles to obtain a serum,[21] and manipulating fluid flow.[22] Even with a well-developed library of techniques available, there

are more intricate challenges that must be addressed to produce a fully developed sample-to-answer system.

LoD devices are capable of performing complex protocols, but integrating multiple large machines that perform different steps for a test onto a small system, developing gas and liquid impermeable valves to prevent cross contamination and premature reagent release, and the dependence on rotational speeds are challenges that must be addressed. Active valves, such as ice valves,[23] wax valves,[24] and optically actuated valves,[25] require external energy sources for actuation but are effective in manipulating fluids. Electrolysis[26] and thermo-pneumatic pumping[27] are active pumping techniques that also require external energy sources for actuation and allow for more complex fluid sequencing. Integrating droplet production onto LoD devices is challenging to accomplish but can be advantageous.

The LoD platform allows for multiplexing and sample processing, has a broad range of applications, and is scalable to handle milliliter to picoliter volumes.[16,28] Combined with the shorter diffusion length and high throughput potential of droplet microfluidics, it is possible to develop a versatile diagnostic device. The biggest challenge to integrating droplet microfluidics onto microfluidic disks is the need to understand how droplet generation is achieved on LoD systems, which this work begins to address.

1.3 Theory of Droplet Generation

The highly complex physics of droplet generation in microfluidics is not fully understood, but there is enough information to implement droplets on microfluidic devices successfully.[29] The preferred method for investigating droplet generating regimes is analysis by dimensionless numbers.[30] Rather than producing a fully predictive model, the scope of this work provides the

foundation needed to aid exploration in this complicated field of study. Dimensionless numbers are presented and explained, alongside pressure gradients and volumetric flow rates, to establish basic conditions required to produce droplets and manipulate droplet size on CDs.

There are two techniques for producing droplets: T-junction shearing and hydrodynamic flow focusing. The first technique, the T-junction, has a straightforward geometry. Just as it sounds, the junction forms a "T" shape with an immiscible two-phase inflow, a continuous organic phase and a dispersed aqueous phase, and an outflow. As shown Figure 1, the T-junction has the continuous phase flowing in a straight vector across the top of the "T" shape. The dispersed phase intersects with the continuous phase perpendicularly, forming the base of the "T" shape. The dispersed phase is flown into the continuous phase, necks, and is sheared away. Necking and shearing are achieved by inertial forces of the oil phase flowing into the protruding water column. The surface tension of the hydrophilic dispersed phase is competing with the shear stress, resisting water from breaking off of the parent stream. The shear stress constantly pushes the protruding dispersed phase, collapsing the neck closer to the downstream edge of the inlet. Once the neck of the protrusion has collapsed, a droplet is broken off and formed.[31,32] This process repeats in a sinusoidal pattern as long as the volumetric flow rate of the dispersed phase (Q_{water}) is not much greater than the volumetric flow rate of the

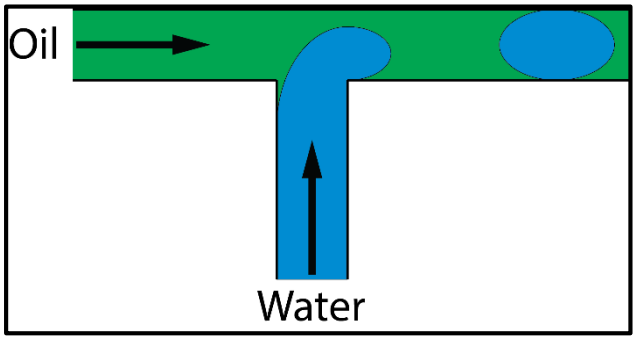

Figure 1. A schematic of a T-junction. Oil is flowed from the left to the right across the top of the "T." Water is injected from the bottom, or base of the "T," into the oil phase. The surface tension holding the water together is competing with the shear stress of the oil flow. In this case, the shear stress dominates and pushes the tip of the protruding water column. As a result the water column necks and collapses against the downstream edge of the injection channel, producing a droplet.

continuous phase (Q_{oil}). Previous research regarding the T-junction technique has been done on the LoD platform by Meghan Cozzens.[33] In short, this method was not chosen for analysis in her work or in this work as it was difficult to get highly monodispersed droplets of a constant size in the same trial. This can mainly be attributed to the manufacturing techniques used as well as the rotational pseudo-forces of the LoD platform. For more information, the reader is referred to the S. L. Anna and G. M. Whitesides research groups.

The second technique for droplet generation is hydrodynamic flow focusing. The geometry for this technique has four channels intersecting, as shown in Figure 2. The dispersed phase and continuous phase channels are oriented to direct the flow perpendicular to each other. Together, the channels form the shape of a "t" instead of a "T." This produces a precisely controlled nozzle from which the dispersed phase "drips." One additional parameter is important for this flow focusing feature (FFF) to produce droplets: the geometry of the outlet channel.

The outlet channel geometry plays an integral role in droplet break off. Tan et al. explained that there must be a concise point of maximum flow velocity in order to generate droplets. This condition is necessary to focus the shear stress from the organic phase to a single point. So rather than distributing the shear stress across the entire interface between the phases, the geometry of the feature concentrates it on a single line across the aqueous phase. [34] A viscous force, which is a result of the immiscible fluids interacting on an interface between them, is also exerted onto the aqueous phase by the organic phase. Without focusing the inertial energy of the bulk flow, the viscous force dominates and pulls the dispersed phase to flow alongside the continuous phase in a phenomenon called co-flow. To avoid co-flow and achieve an optimal focal point for the fluid velocity, the entrance to the outlet channel must be the narrowest part exiting the intersecting. If the diameter of the outlet is maintained too far beyond the entrance

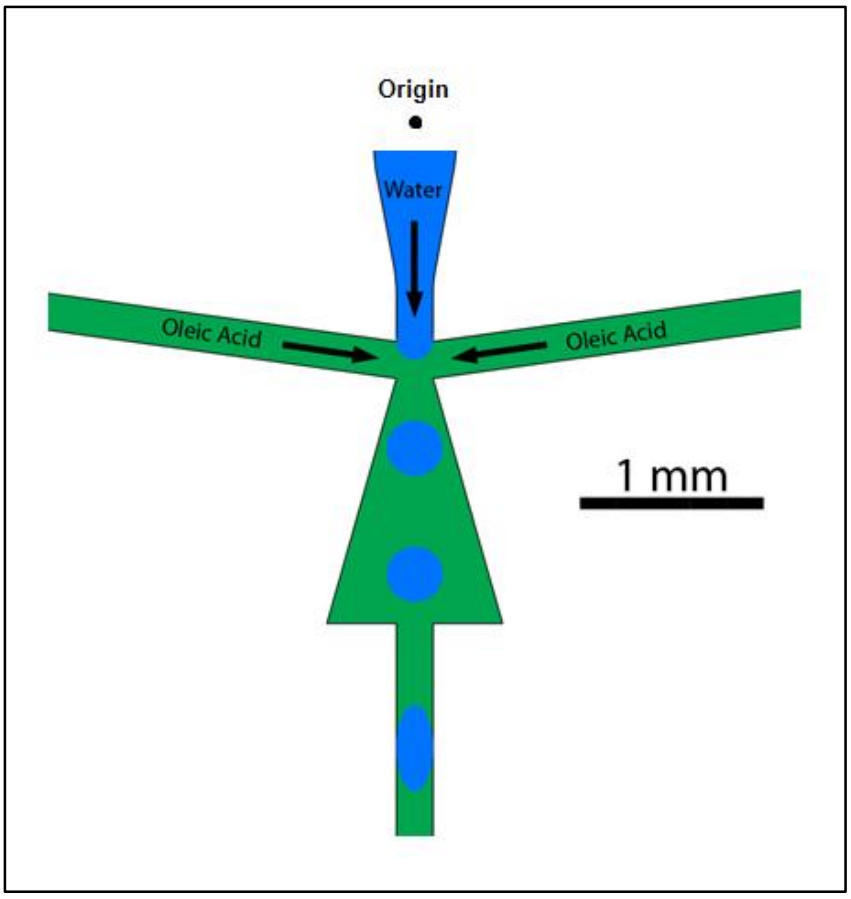

Figure 2. A schematic of the hydrodynamic flow focusing feature used in the experiments of this work. In LoC chips, all four of the channels are typically oriented such that the aqueous and organic phase flows are perpendicular to each other. However, due to the circular nature of the rotational pseudo-forces, the channels must be offset to direct the bulk of the flow toward the radius of the disc. Oleic acid is pumped through the two side channels, and water is pumped through the centered channel to the intersection. When the flows meet, the oleic acid pinches the water stream together due to inertial forces. The triangular shape of the outlet channel focuses the velocity of the flow of both phases is down to a single point at the entrance to the outlet channel. The water stream necks and collapses at this point of maximum flow velocity to form droplets.

and onto the rest of the outlet channel, droplet break off is much less likely to occur. By modifying the geometry of the channels to narrow or widen the focal point of the shear stress, it is possible to manipulate droplet size.[30] The flow simulations completed by Tan et al. explain this concept in further detail and the ideas of that article were applied to the fluidic design of the CDs run in this work.

To investigate the effect of channel geometry on droplet size, Haeberle et al. used dimensionless numbers. Capillary and Weber numbers are the most important for interpreting droplet generation for LoC devices. Capillary number is the ratio of viscous forces versus surface tension acting across the interface between the two immiscible phases. It is given in Equation (1):

$$Ca = \mu_c \overrightarrow{v_c} / \gamma \qquad (1)$$

where μ_c is the dynamic viscosity of the continuous phase, $\overrightarrow{v_c}$ is the flow velocity of the continuous phase, and γ is the interfacial tension between the two phases. While channel geometry was not altered during the course of this study, the interfacial tension was changed by switching between oleic acid (Sigma-Aldrich W281506) (γ = 15.6mN/m) and light mineral oil (Sigma-Aldrich 330779) (γ = 52.93mN/m).[35,36] Weber number represents the ratio of inertial forces to surface tension forces between fluids. It is given in Equation (2):

$$We = \rho_d v_d l^2 / \sigma \qquad (2)$$

where ρ_d is the density of the dispersed phase, v_d is the velocity of the dispersed phase, l is the characteristic geometry of the dispersed phase (i.e. the hydraulic diameter of the discontinuous phase nozzle). These dimensionless numbers are important in understand how droplets are formed.

Studies have shown that when the We and Ca numbers are less than their crucial values, We_{crit} and Ca_{crit} respectively, droplet generation occurs. The critical capillary number was found empirically to be roughly 0.1 when droplet production happens.[29] Above these critical values, droplets break off from the parent stream due to the optimal balance of forces in a FFF. Several parameters must be considered when designing the fluidic features to produce droplets. The first is the flow rates of the two phases. The second is the physiological properties of the fluids, such as density, viscosity, surface tension, and interfacial tension. Third is the geometry of the FFF, which includes the channel depth, width, orientation, and shape. A model for predicting droplet

formation based on these parameters and characterized by these dimensionless number would be very beneficial for the field of centrifugal microfluidics. This work focuses on characterizing the different flow regimes to help develop a model.

There are three flow regimes that characterize the interactions between the different forces for producing droplets. The most sought after is the "dripping regime," which is the zone that droplets are made in. In general, as long as $Q_c \geq Q_d$, the system is in the "dripping regime." There is a "co-flow regime" in which the phases flow parallel to each other and no droplet break off occurs. If the outlet channel is long enough, it is possible to have "jetting," which is when droplets are produced at the end of a long thread of water as a result of turbulence downstream from the FFF. Co-flow generally occurs when the continuous phase flow rate is less than the dispersed phase flow rate such that $Q_c < Q_d$. The "no flow regime" is when no water protrudes from the nozzle and no droplets or jetting is allowed. This blockage is a result of having a continuous phase flow rate that is significantly higher than the dispersed phase flow rate such that $Q_c >> Q_d$. Figure 3 summarizes the events and flow rates of these regimes.

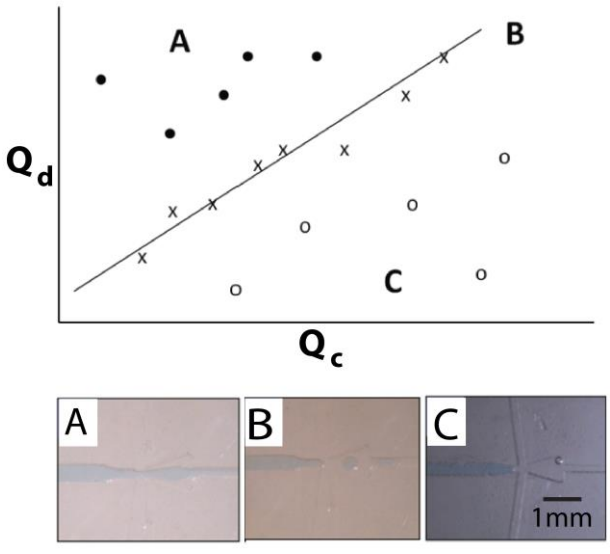

Figure 3. A graph depicting the three different flow regimes for droplet microfluidics accompanied by correlated images from CD experiments of this work. **A** is the "co-flow regime" where $Q_c < Q_d$. The two phases flow in parallel and jetting can occur under this condition. **B** is the "dripping regime" where $Q_c \geq Q_d$. Droplet production occurs under this condition. **C** is the "no flow regime" where $Q_c >> Q_d$. No water is injected into the system under this condition.

Many studies have found that the ratio between the volumetric flow rates of the two phases affects the size of droplets.[31,37–39] The ratio is calculated as

$$\varphi = Q_c/Q_d \qquad (3)$$

The flow rates can be affected by a number of parameters, including fluid viscosity, contact angle, and channel geometry. Figure 4 highlights the important aspects covered in this section.

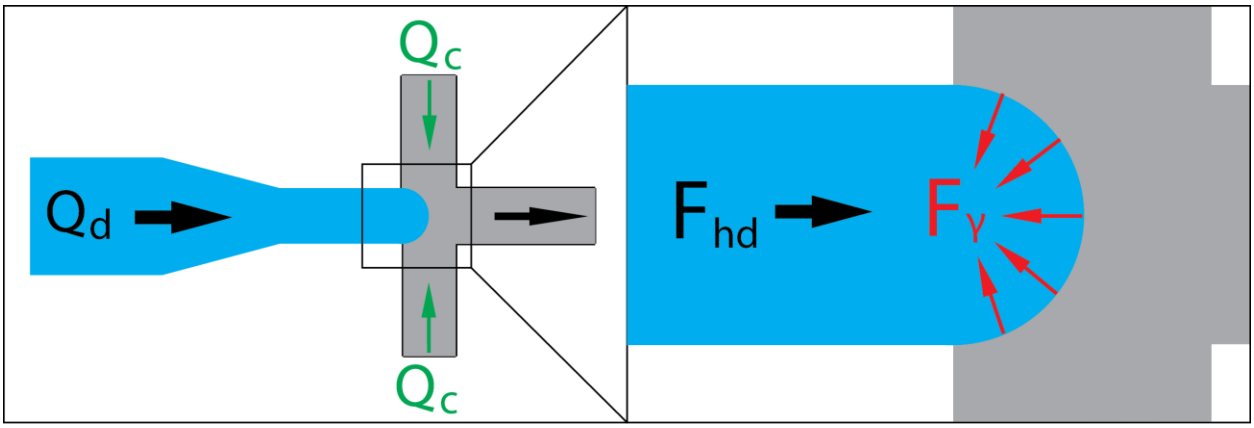

Figure 4. Flow rates and forces in a flow focusing feature. (left) A schematic of the FFF on a CD is shown with the droplet generation nozzle, flow of the dispersed phase, Q_d, and flow of the continuous phase, Q_c. (right) A free body diagram of the penetrating dispersed phase tip is shown with the hydrodynamic force, F_{hd} (this represents the pressure injecting the dispersed phase), and the surface tension force, F_γ (this represents the interfacial tension between the two phases and the surface tension of the dispersed phase).

CHAPTER 2: Integrating Droplets onto Centrifugal Microfluidic Platforms

2.1 Droplet and Bubble Generation on CDs

Droplet emulsions and bubble generation have been integrated onto the LoD platform by Haeberle et al. and Chakraborty et al. respectively.[30,40] Haeberle et al. was the first to successfully demonstrate droplet generation on CDs, characterizing droplet formation and exploring several applications. In order to achieve droplet production, there is a set of conditions to which the fluidic system must comply. Haeberle used dimensionless numbers to explain these conditions and which flow phenomena is allowed with such conditions. The relationship between droplet size and parameters, including angular velocity and flow focusing geometry, were explored. This is significant in that changing droplet size without physically changing the channels could potentially lower production costs. Techniques such as droplet splitting, mixing two aqueous solutions in droplets, and droplet sedimentation are also demonstrated. Droplet splitting, or fission, was achieved by implementing a second flow focusing feature downstream from the first. At the optimal angular velocity, this additional junction caused droplets to split into smaller segments. At higher angular velocities, satellites are produced. Droplets containing a 1:1 ratio of ink and deionized (DI) water were successfully mixed, providing further evidence to shorter diffusion durations in droplet fluidics. Droplet sedimentation was completed, separating the droplets from some of the continuous phase. While liquid droplets are the focus of this work, it is important to consider gaseous bubbles as well.

Chakraborty et al. replaced the liquid dispersed phase with a gas to produce microbubbles on CDs. The bubbles were produced in the same manner using a flow focusing feature to pinch off bubbles using an organic continuous phase. Maintaining the same channel geometry

throughout the experiments, bubble production regimes, bubble sizes, and bubble production rate were characterized in relation to the angular velocity of the device.

Continuing from the accomplishments of Haeberle et al. and Chakraborty et al., this work characterizes droplet formation with respect to several components of the LoD platform. Contributing to these factors are the geometry of the flow focusing feature, the height of the fluid columns, the angular velocity of the CD, and fluid properties (specifically interfacial tension between the phases and viscosity of the phases). These parameters provide insight into controlling droplet size. Using different fluidic designs, angular velocities, and organic continuous phase solutions, an in depth analysis of droplet generation was executed.

2.2 Challenges of Integrating Droplets onto CDs

There are numerous challenges for integrating droplet microfluidics onto the LoD platform. One problem is that the highly complex physics of droplet generation is not fully understood despite many groups studying this field. As such, guidelines have been empirically determined through the capillary and Weber numbers to predict the fluidic state of a system given certain parameters. So far, this has only been applied to LoC devices. Special considerations must be made in order to translate droplet microfluidics to LoD devices, including the use of an additional dimensionless number and the rotational pseudo-forces of the platform.

Droplet generation may also be dependent on the Bond (Bo) number due to the rotational effects on centrifugal microfluidic systems. The Bo number is defined as the ratio between gravitational forces and surface tension forces. Since the centrifugal microfluidic system has artificial gravity from the rotational pseudo-forces, the Bo number must be examined. It is given in Equation (4):

$$Bo = \rho_D a l^2/\gamma = A_n(\rho_d - p_c)\omega z/\gamma \qquad (4)$$

where ρ_D is the difference between the densities of the dispersed phase and continuous phase, a is the acceleration due to the artificial gravity generated by the centrifugal pseudo-force (ωz), l is again the characteristic geometry of the channels ($l^2 = A_n$), the cross-sectional area of the nozzle), and γ is again the interfacial tension between the continuous and dispersed phases. If the Bo number is high, the gravitational forces (i.e. centrifugal force, Coriolis force, etc.) dominate. If the Bo number is low, the surface tension forces dominate. One future area of research would be to fully characterize the Bo number on centrifugal microfluidic devices and compare those values to those from LoC chips.

LoC devices are able to control the pressure and flow rate of different fluids independently. LoD devices provide the same rotational pseudo-forces on the radius of entire platform, thus preventing individual fluid pressure and volumetric flow rate changes in the middle of an experiment. The fluid column heights and channel resistances must be determined prior to fabrication. Thus, it is important to understand the relationship between these parameters and the pressures and volumetric flow rates as this also affects droplet break off and size.

Due to the unique pumping mechanism in CD microfluidics, where both fluids are controlled by the application of centrifugal force, it is not possible to independently vary Q_d and Q_c during an experiment in order to tune droplet production. The volumetric flow rate of a particular phase, Q_i, may be changed by increasing or decreasing the angular velocity (ω) according to:

$$Q_i = \rho_l \omega^2 \bar{r} \Delta r/R \qquad (5)$$

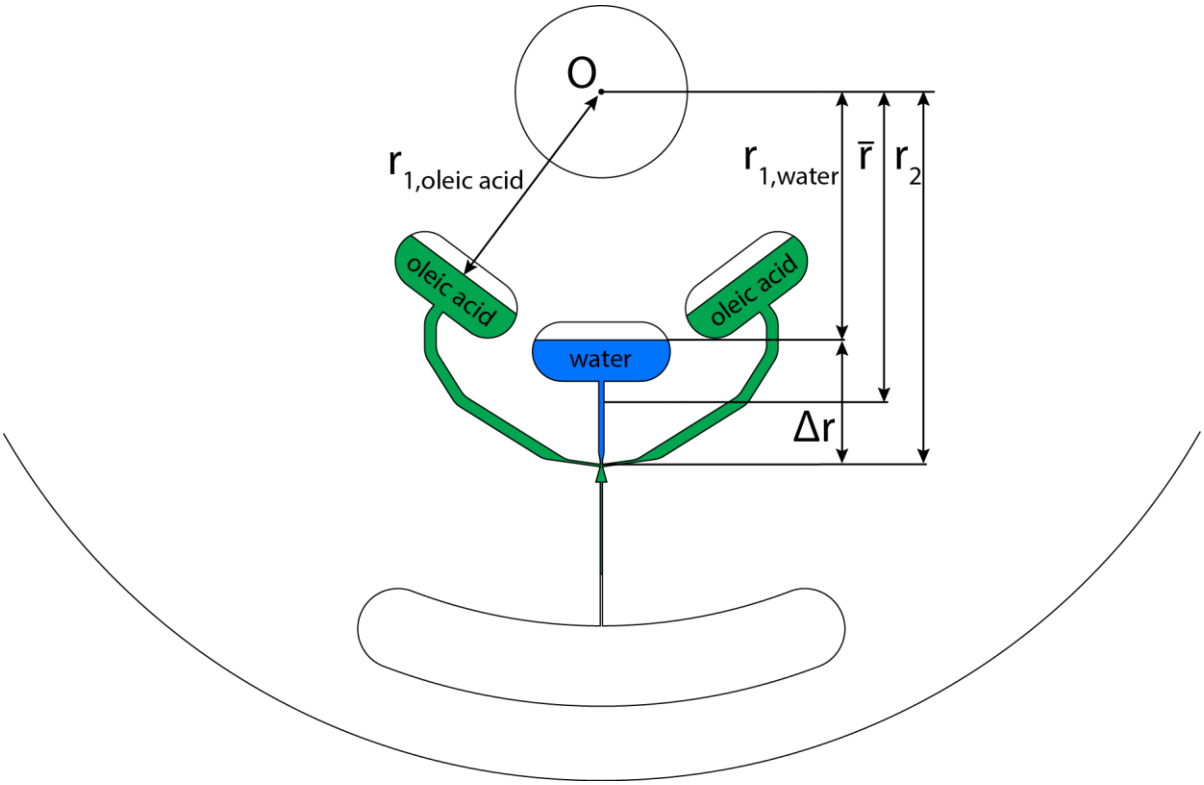

Figure 5. A schematic of the primary fluidic design used for the channels and chambers on the CDs. Important radial positions relevant to the pressures driving fluid flow are noted from left to right: $r_{1,oleic\ acid}$ is the radial position of the oil meniscus closest to the center of the disc, $r_{1,water}$ is the radial position of the water meniscus closest to the center of the disc, Δr is the difference in heights between the meniscus of the fluid closest to the center of the CD and the meniscus of the same fluid closest to the perimeter of the CD, $\bar{r}$ is the mean fluid height, and r_2 is the radial position of the meniscus closer to the perimeter of the CD (in this case the radial position of the nozzle is r_2 as it is the point of interest for fluid pressure and velocity).

where ρ_l is the density of the observed liquid, ω is the angular velocity of the disk, $\bar{r}$ is the average fluid column height from the origin of the disk, Δr is the difference in radial positions of the menisci of a single fluid, and R is the fluidic resistance of the channels given in Equation (6):

$$R = \sum_i 32\mu L_i/(A_{cs,i} \times D_{h,i}) \qquad (6)$$

where L_i is the length of the observed channel, $A_{cs,i}$ is the cross-sectional area of the channel of a certain phase, and $D_{h,i}$ is the hydraulic diameter of the channel ($4A_{cs,i}/P$ where P is the wetted perimeter of the channel). The volumetric flow rate ratio, φ, is constrained by the following equation, which is obtain by substituting equations (5) into Equation (3):

$$\varphi = Q_c/Q_d = \frac{(\rho_c \omega^2 \bar{r} \Delta r)/R_c}{(\rho_d \omega^2 \bar{r} \Delta r)/R_d} = (\rho_c \bar{r} \Delta r) R_d / (\rho_d \bar{r} \Delta r) R_c \qquad (7)$$

Note that the term ω from Equation (5) drops out of the simplified relation. Thus, the flow rate ratio, and, therefore, the droplet size, cannot be varied simply by changing the angular velocity, ω. That is not to say that ω plays no role in controlling the conditions needed for droplet production. It is just not the dominant factor in manipulating droplet size. For a fluidic system of particular ρ_c, ρ_d, μ_c, and μ_d values, it is possible to vary the fluidic resistance of the two channels to control φ and, therefore, the droplet size. As shown in Equation (6), varying the channel lengths, cross-sectional areas, or both can alter the φ and droplet size.

Interfacial tension values leads to knowing critical values of the previously mentioned dimensionless numbers (Ca, We, and Bo numbers). Knowing these critical values provides insight into the physics of droplet generation. The difficulty here is that there is a limited amount of available data from the literature regarding the interfacial tension of commonly used solutions for droplet emulsions. Thus, oleic acid and light mineral oil were chosen as they have been studied extensively, providing a substantial amount of information from the literature, and they are commonly used in producing droplets on LoC platforms.

Returning to the end of Section 1.3, specifically the part covering the balance of forces at the nozzle of the FFF with Figure 4, examining the traits of the dispersed phase at a point just

prior to droplet break off provides information on how the hydrodynamic forces and surface tension forces interact on CDs. Constructing a force balance on the penetrating tip of the dispersed phase allows for the calculation of the interfacial tension between the two phases.

There is a balance between the centrifugal force (the dominant component of the hydrodynamic force) that pumps the dispersed phase through the channel, to the droplet-generation nozzle, and the surface tension force, or Laplace pressure force (P_γ). The hydrodynamic force at any radial position on the CD is usually represented by the meniscus pressure, $P_{meniscus}$, which acts across the cross-sectional area of the nozzle, A_{cs}. This counteracting Laplace pressure force is given in Equation (8):

$$P_{meniscus}A_{cs} = P_\gamma A_{cs} \qquad (8)$$

The cross-sectional area for each of these forces is equal in the designs, so the pressure balance equation is left. Substituting in the appropriate equations for each pressure gives:

$$\rho\omega^2\bar{r}\Delta r = 4\gamma \sin(\theta_c)\,/D_h \qquad (9)$$

where θ_c is the equilibrium contact angle. Solving for the interfacial tension, γ, gives:

$$\gamma = \rho\omega^2\bar{r}\Delta r D_h/4\sin(\theta_c) \qquad (10)$$

Thus, the value of the interfacial tension between the chosen aqueous and organic phases can be determined by knowing the geometry of the disc, the angular velocity ω, and the equilibrium

contact angle θ_c. For a more precise determination, it is helpful to calculate θ_c at various values of ω and average the calculated values for γ.

2.3 Technology Comparison

New microfluidic products have implemented droplet technology for research applications. One such product by Rain Dance Technologies™ uses a high throughput picoliter droplet emulsion system, which was launched in 2014. It is an automated benchtop digital PCR device called RainDrop®. The throughput is exceptionally high, running 80,000 PCR reactions per second and addressing the problem of generating results faster. In fact, the device is at least 500 times faster than current PCR methods. In order to achieve such swiftness, the device is capable of multiplexing several probes of varying concentration across eight detection channels while producing monodispersed, uniform droplets. This multiplexing can be expanded further with different fluidic setups. The detection unit of RainDrop® monitors reactions in real-time with a lower limit of detection (LLOD) around one part per million. Comparable to the LoD platform, RainDrop® is a closed system, with all reagents and emulsion fluids sealed from the environment and all of the fluidics manipulated automatically without the need for extra pipetting. RainDrop® microfluidic chips are single use, similar to the disposable disks of the LoD platform. Finally, Rain Dance Technologies™ has a small database for applying digital PCR to research fields using their products.[7]

It is possible for the LoD platform to compete with the products developed by Rain Dance Technologies™, however, more research in this area will be necessary. There are some advantages to using centrifugal microfluidic disks over RainDrop®. One advantage is having a completely closed system. Another benefit is portability, as RainDrop® has a larger desktop

format. These droplet emulsion platforms have a competitor that uses a different approach to liquid handling.

An up and coming approach to droplet technology is Electrowetting on dielectric (EWOD) based microfluidic chips, which present a compact, single phase alternative to droplet emulsions. EWOD-based microfluidic chips share many similar advantages to the standard droplet emulsion methods, including the low reagent consumption, higher reagent mixing efficiency, and shorter reactions times.[4,41,42] It is also an attractive alternative to the standard droplet emulsion methods due to its portability and modularity. Rather than having fluidic channels to direct fluid flow, a reservoir with a dielectric surface is utilized to break off small portions of sample for mixing, heating, detection, and other analytical procedures. To superficially explain the concept, the surface of a polymer chip is coated with a dielectric material, which is connected to a voltage supply. The amount of voltage applied to the dielectric material alters the surface tension interaction between the liquid and the solid. For example, a hydrophobic dielectric material initially repels a hydrophilic liquid. Once a voltage is applied to the dielectric material, the surface becomes more hydrophilic and is able to be wetted by the hydrophilic liquid. The dielectric surface is split into multiple segments such that a coordinated series of voltages changes can "pull" droplets to different steps on the chip. Even though these chips are versatile and can detect multiple probes simultaneously, there is no method for multiplexing available for EWOD-based chips that is able to compete with that of droplet emulsion platforms. Thus, the biggest disadvantage of using EWOD chips is low throughput.

LoD devices are the middle ground between LoC and EWOD devices for droplet microfluidics. LoC droplet emulsions have a very high throughput, can be multiplexed, and is mostly a closed system. However, to achieve such a high throughput and house external pressure

pumps, the platform generally has a larger footprint. Meanwhile, EWOD-based chips are easily portable with a compact format, but have a low throughput. The LoD platform is a completely closed system and has a smaller footprint than LoC systems due to the use of a motor to drive fluid pumping rather than syringe pumps. EWOD-based chips are smaller with a format as small as cell phones. LoD systems have a higher throughput than EWOD-based chips, but must be explored more to compete with LoC systems in this regard. How droplets emulsions are generated on centrifugal microfluidic disks must be explained to achieve this goal.

CHAPTER 3: Characterization of Droplet Generation on a Centrifugal Microfluidic Platform

3.1 Materials and Methods

There is a wide variety of materials and manufacturing techniques used to make microfluidic CDs. One must consider the applications and testing procedures when deciding which materials and manufacturing methods to use. Parameters to consider include but are not limited to testing duration, maximum angular velocity, maximum liquid volume in a single chamber, reactions between the CD materials and the chemicals used, inhibitors in the materials, maximum heating temperature, and heating duration.

To start, thermoplastics are the most common materials as they are cheap, easy to prototype, and easy to mass manufacture with hot embossing or injection molding techniques. The UCI BioMEMS group mostly uses polycarbonate (PC) as it is scratch resistant, durable, easy to mill, and slightly cheaper than other plastics. It is slightly hydrophilic with a θ_c of roughly 82°.[43] The biggest problem with using PC is that it has autofluorescence, meaning that it has its own fluorescence spectrum providing a substantial amount of background noise during fluorescent studies. The MIMEMS group of Malaysia prefers poly(methyl methacrylate) (PMMA) as it has a weaker autofluorescence spectrum and is more optically clear than PC. Other minor advantages are that it is more readily available and cheaper than other plastics in that region. The disadvantages here are that PMMA is brittle, prone to scratches and chipping, and requires a fair amount of experience to be milled properly. PMMA is more hydrophilic than PC with a θ_c of roughly 68°.[44] Polydimethylsiloxane (PDMS), which is very hydrophobic with θ_c of roughly 107°, was used in the past to manufacture fluidic structures. In a process called soft

lithography, the PDMS mixture would be molded using a silicone positive mold and then cured to harden. The PDMS was then exposed to oxygen plasma treatment, temporarily altering its surface to be much more hydrophilic, and bonded to glass. The entire chip was mounted onto a custom spin chuck and rotated to pump fluids. Using plastics was faster to prototype and scale up to mass manufacturing, thus the shift to using PC and PMMA. PC and PMMA have been studied more extensively than other plastics, and they are the most common plastics used in production today. For these reasons PC and PMMA have been used by research groups extensively.

Milling plastics is a common method for making prototype channels and chambers on CDs. In the case of PC this is the only method to use without using injection molding, which is extremely expensive on a small scale. PMMA, on the other hand, can be cut using a laser if the material is thin enough. Because PMMA is more brittle and denser than PC, carbide tools are needed to provide the tools extra structural strength and prevent breaking during use. Carbide tools are noticeably more expensive, resulting in laser cutting as the preferred method for cutting PMMA. PC cannot be cut using a laser as the chemical interaction between the laser and PC during ablation produces a toxic byproduct. Once the plastic layers are cut, they must be bonded together.

Pressure sensitive adhesive (PSA) or foil is the most common material used for bonding plastic layers. In a mass manufacturing setting, the plastics would be heated to the glass transition temperature and pressed together. In a research setting, this method is not practical. PSA comes in a variety of thicknesses, adhesion strength, and surface chemistry. There is also the choice between medical and non-medical grade adhesives. The thickness determines the channel height if the channels are cut into the PSA rather than the plastic layers. The adhesion strength must be determined by the spin and heating parameters. For example, the adhesive

should hold the CD together at the maximum angular velocity without any signs of leaking, and it should not melt during a heating protocol. The composition of the PSA is also important. PCR inhibitors have been found in general purpose adhesives, but special PSA types are made for this problem. FLEXcon, 3M, and Alcon are just a few of the vendors that produce adhesives used by CD microfluidics research groups.

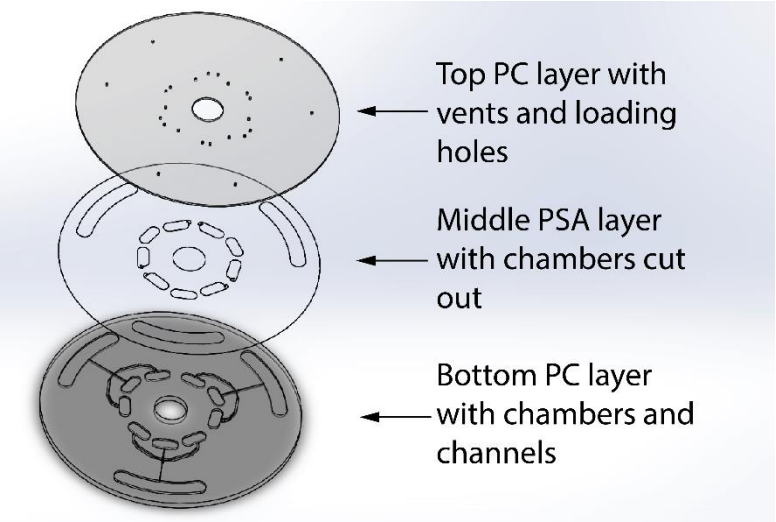

Figure 6. Exploded view of a three-layer microfluidic CD. The top layer is 1mm thick PC with vent and loading holes drilled into it. The middle layer is the adhesive with the chambers and center hole cut out. The bottom layer is a thicker 3mm PC with channels and chambers milled into it.

For this study, 1mm and 3mm thick PC sheets (McMaster-Carr, CA, USA) were used to form three-layer microfluidic CDs. Figure 6 shows an exploded view of a full CD with the vent and loading holes in the top layer, the PSA (FLEXcon, MA, USA) in the middle to bond the hard plastic layers together, and the fluidic channels and chambers in the bottom layer. The top PC layer was milled using a computer-numerical control (CNC) mill (T-tech, GA, USA- QuickCircuit 5000). The middle layer of PSA was cut using a plotter (Graphtec, Japan – Graphtec CE-2000). The bottom PC layer was milled using a 2.5D CNC mill (Roland, CA, UA – MDX-40). A roll press was used to activate the PSA and bond the PC layers together.

Loading the chambers for this two phase system was not straightforward. The water with food dye was loaded first into the center chamber close to the center of the disk using a pipette.

Once the chamber was full, extra pressure was exerted to push the water to the flow focusing feature, but did not burst. By pushing the water as close to the FFF as possible, it reduces the air bubble volume that gets trapped between the oil and water phases at the beginning of the trials. The oil was loaded into the two offset chambers closest to the center of the disk next, and, due to the interaction between the oil and the plastic, it wetted the channels easily. The loading holes are then sealed off to prevent leaks and the disk is mounted onto the spin chuck of the spin stand.

Several organic phases were explored to find the optimal conditions for droplet generation. Oleic acid (OA) (Sigma-Aldrich W281506) with a $\gamma = 15.6 mN/m$[35], $\mu = 38.8 Pa*s$, and $\rho = 0.89 g/mL$ was used. Droplets were produced successfully when paired with De-ionized (DI) water with properties $\mu = 1.0020 Pa*s$, $\rho = 1000\ g/mL$, and $\sigma = 72.8 mN/m$. Silicone oil (Sigma-Aldrich) with properties $\gamma = 39.8 mN/m$[45], $\mu = 5 Pa*s$ to 1*10^6Pa*s, and $\rho = 0.90+ g/mL$ was used to no avail as the available viscosities were too high to allow the phase to flow. Heavy mineral oil (Sigma-Aldrich 330760) with properties $\gamma = 30.5 mN/m$[46] and $\rho = 0.862 g/mL$ was also used, but the viscosity again was too high to allow the phase to flow in the channels. Light mineral oil (LMO) (Sigma-Aldrich 330779) of properties $\gamma = 52.93 mN/m$[47], $\mu = 0.5 mPa*s$, $\rho = 0.838 g/mL$ was used. Droplets were generated successfully when paired with DI water. Methoxy-nonafluorobutane (HFE) (Sigma-Aldrich 65139) was the last organic phase solution tested. Its properties are mostly unavailable, but the density was 1.52g/mL. This solution drained quickly at angular velocities <10.5 rad/s, making it impractical to work with for CD microfluidics since the burst frequency of water with these smaller channel dimensions is a minimum 31 rad/s. After these initial trials, oleic acid and light mineral oil were chosen to study the impact of interfacial tension on droplet generation and size on CDs. These two solutions have been studied at length, providing a large library of information to draw from, and they are

commonly used in droplet microfluidic experiments. No surfactant was used for any of the tested organic phase solutions. In most cases, adding surfactant would require a materials study beyond the scope of this work. Future experiments could be based on using surfactants and their effects on surface tension during droplet formation.

After preparing a CD, it is placed onto the aluminum spin chuck of the spinstand. The spinstand testing platform is equipped with a brush servomotor, camera (Basler avA1000) with a macro lens (Zeiss), strobe illumination lights (PerkinElmer, MA, USA) and a user interface generated with ToolPaq. The software package (CD Imager K1000, Key Lead Solutions, Inc.) the user is able to control the camera parameters, including strobe exposure, frequency, contrast, gamma, and other imaging settings. The servo motor allows rotational speeds of up to 1570 rad/s. A high speed camera is used to capture still frame images of the disc once per rotation, at a resolution of 658 x 492 pixels. A laser and reflector system mounted onto the platform synchronizes the camera, strobe light, and motor to capture the events happening on the rotating disk. The images are saved as BMP files and then compiled into an AVI video file using ImageJ (NIH, Bethesda, MD).

Fluid column heights were measured and used to calculate the hydrostatic pressures, volumetric flow rates and volumetric flow rate ratios. These values were then compared to droplet size and dimensionless numbers to analyze any correlation between them.

3.2 Predicting Flow Regimes

Droplet generation has been integrated onto microfluidic CDs in the past. Parameters such as angular velocity and dimensionless numbers have been investigated in regards to droplet

size. What has not been explored is a set of conditions that allow droplet formation. This work focuses on the geometry of the FFF and the pressure ratio determined by the fluid column height.

$P_{meniscus}$ is the pressure exerted by the fluid column in response to centrifugal force pushing the fluid downstream. Referring back to Figure 5, Equation (11) describes $P_{meniscus}$ where ρ_i is the density of the observed liquid, ω is the angular velocity, $\bar{r}$ is the distance from the center of the disc to the average fluid length, and Δr is the difference between the upstream and downstream menisci of the observed fluid column:

$$P_{meniscus} = \rho_i \omega^2 \bar{r} \Delta r \qquad (11)$$

What is different from common microfluidic devices, is the fact that there are two liquid phases. Instead of having just one aqueous phase, there is also an organic phase. These immiscible fluids add complexity to the system, and now more than one $P_{meniscus}$ must be calculated. P_{water} and P_{oil} have the following equations:

$$P_{water} = \rho_{water} \omega^2 (r_{1,water}^2 - r_2^2)/2 \qquad (12)$$

$$P_{oil} = \rho_{oil} \omega^2 (r_{1,oil}^2 - r_2^2)/2 \qquad (13)$$

Where $r_{1,water}$ is the distance from the center of the disk to the upstream meniscus of the water column, $r_{1,oil}$ is the distance from the center of the disk to the upstream meniscus of the oil column, and r_2 is the nozzle, since that is the point of interest for the pressure value.

A number of studies demonstrate droplet formation at $\varphi \geq 1$ when the oil phase flows at the same rate or more than the water phase.[31,37–39] The critical value of φ is assumed to be 1. Since Q is proportional to P, the assumption of $P_{water} = P_{oil} = 1$ is made, giving Equation (14):

$$\rho_{water}\omega^2(r_{1,water}^2 - r_2^2)/2 = \rho_{oil}\omega^2(r_{1,oil}^2 - r_2^2)/2 \qquad (14)$$

The angular velocity, ω, is cancelled out and all but $r_{1,water}$ and $r_{1,oil}$ are constant as r_2 is shared between the two phases. Choosing to have $r_{1,water}$ as the independent variable during experiments, Equation (14) is solved for $r_{1,oil}$, giving Equation (15):

$$r_{1,oil} = \sqrt{r_{1,water}^2 * \left(\frac{\rho_{water}}{\rho_{oil}}\right) + r_2^2 - r_2^2 * \left(\frac{\rho_{water}}{\rho_{oil}}\right)} \qquad (15)$$

Setting $r_{1,water}$ to arbitrary values between 15mm and 35mm, due to the design of the disk, the theoretical trend line is established. The slope can be considered linear since the range for $r_{1,water}$ is so small.

Experiments were run with 100um channels initially using oleic acid as the continuous phase. The $r_{1,water}$ and $r_{1,oil}$ values were recorded as BMP file image stacks using the previously detailed spin stand. The angular velocity was increased slowly until the first speed in which droplets began forming. Once the intervals between droplets became larger (1 droplet per second), the angular velocity was increased by 2 rad/s. This process was repeated until the loading chambers were empty. This process was repeated for the other samples as well. By measuring the surface area of liquid missing in the chambers at the start and end of each trial

using ImageJ, the volume could be found to calculate the volumetric flow rate. Droplet sizes were also measured using ImageJ. Figure 7 shows the recorded experimental radial positions of the menisci and the root-mean-square error of the sample. The experimental values fall along the theoretical curve, with the handful of exceptions beneath the curve. The exceptions are because $\varphi > 1$ where the volumetric flow rate of the oil phase is higher than that of the water phase. This difference in flow rate is attributed to a shorter water column. In Figures 7-9, it is important to remember that the smaller the radial position is, the higher the water column is, and, therefore, the higher the pressure is. On the opposite side of the theoretical curve, there are several co-flow values where $\varphi < 1$. The volumetric flow rate of the water phase is too high to allow the inertial

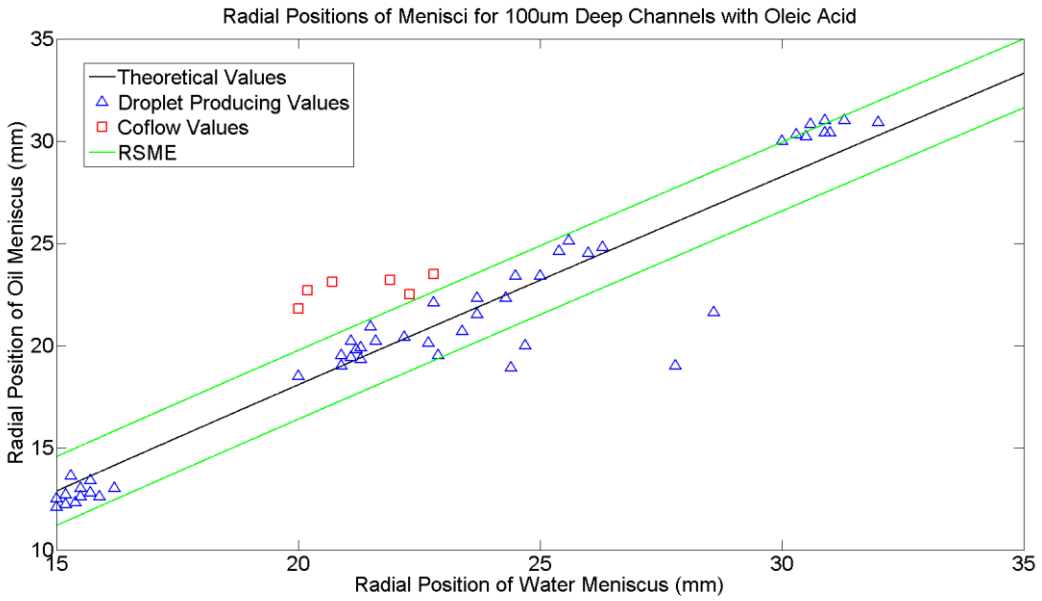

Figure 7. A graph comparing the experimental results and root-mean-square error to the theoretical trend for 100µm deep channels with oleic acid as the continuous phase. Droplet production occurs near or below the theoretical trend line. Co-flow occurs when the flow rate of the dispersed phase is greater than that of the continuous phase. In the graph above, this regime is above the trend line as the radial position of the water is closer to the center of the disk than the radial position of the oleic acid. This correlates with a higher pressure gradient for the water than the oleic acid. The "dripping regime" is in accordance with the literature as there is a shorter transition between the dripping and co-flow regimes than between the dripping and no flow regimes.

forces of the oil phase to pinch of droplets. The RSME lines show the transition boundary where droplets are both being produced and where co-flow occurs. The CD would have to be made much larger than those fabricated in this work in order to study the no flow regime. Anna et al. was able to achieve droplet formation up to $\varphi = 40$ near these channel dimensions.[37] With that comes more complications as the adhesive will have to be changed to a stronger one to accommodate the extra mass and the plastic will begin to bow without air bearings to balance the inertial forces deflecting the disk. Also, by changing the adhesive, the wetting properties are also altered and fluidic validation must be run again.

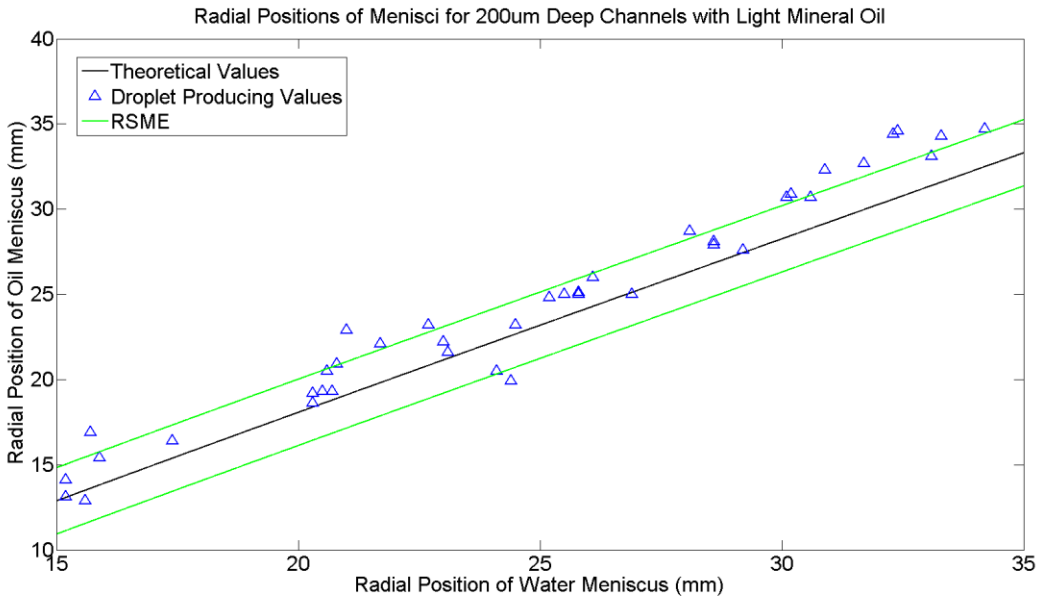

Figure 8. A graph comparing the experimental results and root-mean-square error to the theoretical trend for 200µm deep channels with light mineral oil as the continuous phase. Notice how the spread of the droplet producing values above and below the theoretical trend line is wider than in the previous data set. This is attributed to difficulties in droplet break off due to the interfacial tension of the light mineral oil being significantly higher than that of oleic acid. The shear stress of the light mineral oil flow was attenuated producing larger droplets and a less consistent environment for droplet production. The same trend is found in graphs presented after this.

When LMO was first attempted as the oil phase, it interacted strangely with the adhesive. It behaved as if it sticking to the adhesive. The channel depth was increased to 200µm, allowing the LMO to flow normally. Once the water-LMO trials began, droplets were more difficult to break off. Due to the higher surface tension forces, the inertial energy from the LMO flow had to allow the protruding water tip to extend further than when the disk was run with OA. Once the neck was long enough, the LMO was able to pinch and break off droplets. This created more deviations and spread the droplet producing values away from the theoretical trend line in both directions. Figure 8 reflects this phenomena.

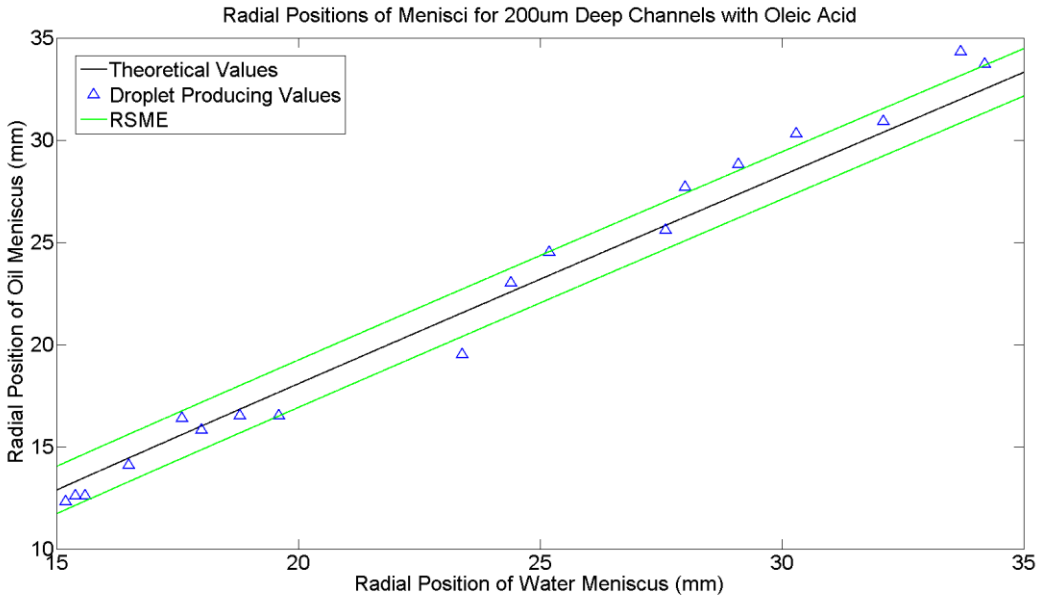

Figure 9. A graph comparing the experimental results and root-mean-square error to the theoretical trend for 200µm deep channels with oleic acid as the continuous phase. Note that the experimental values return closer to the theoretical trend line. This is attributed to the oleic acid having a significantly smaller interfacial tension than the light mineral oil.

To have a stronger comparison between the effects of the interfacial tensions of OA and LMO, the design with 200µm deep channels was run again with OA. The results were consistent with those found previously with the 100µm deep channels using OA as the continuous phase.

Figure 9 shows how much closer the water-OA experimental data follows the trend line than the water-LMO data.

3.3 Dimensionless Numbers, Pressure Gradients, and Flow Rates

As previously stated, dimensionless numbers play an integral role for droplet generation. Droplet generation is dependent on the Ca and We numbers, where the capillary number is the ratio of viscous forces versus surface tension acting across the interface between the two immiscible phases and the Weber number represents the ratio of inertial forces to surface tension forces between fluids. Droplet production may also be dependent on the Bond (Bo) number due to the rotational effects on centrifugal microfluidic systems. This has not been numerically investigated directly in previous work. This study takes a preliminary look at the empirical Bo values, but it is a more thorough investigation must be conducted in future projects to characterize droplet formation properly. It is important to consider these characterization values when analyzing droplet formation and trying to understand when droplet formation will occur on a LoD system.

The data from the experiments were used to calculate the dimensionless number values for each trial. The average values of the different droplet producing experimental samples are noted in Table 1.

Table 1. Average Values of Dimensionless Numbers

	100µm Deep Channels with OA	200µm Deep Channels with OA	200µm Deep Channels with LMO
Average Ca Number	2.668	2.796	17.584
Average We Number	3.448e-6	7.850e-7	6.440e-5
Average Bo Number	5.395	3.760	12.656

No conclusion can be drawn from the data as droplets were produced in all of the trials used to calculate the dimensionless number values. According to several studies about droplets on LoC chips, $We_{crit} < 1$ is in the dripping regime for droplets. In the experiments conducted for this study, droplet production should occur in all of the samples with the exception of the coflow cases. This is found to be true. According to the literature, $Ca_{crit} \sim 0.1$ or any value less than that will most likely produce droplets. The experimental Ca number values are supposedly not low enough to produce droplets, especially in the case of LMO as the continuous phase solution. Both the Ca and We numbers are supposed to be less than their respective critical values to be in the dripping regime, but this is not the case. In all of the cases, Ca > 1, which should not lead to droplet generation despite We < 1 for all cases. In all cases, Bo > 1, which is the Bo_{crit} value. This means that the centrifugal force is dominant and water is allowed to flow. If Bo > 1, no droplet production would be possible as the centrifugal force is not strong enough to push out the water phase. The system at that point would be in the no flow regime. Also of note, the Ca and Bo number values for trials using OA as the continuous phase solution are much lower than the values for trials using LMO as the continuous phase solution. It can be speculated that these conditions led to larger droplet diameters and volumes as shown in Table 2. Droplet volumes were calculated using the equation for finding the volume of an ellipsoid:

$$V = \pi * w_x w_y w_z / 6$$

where w_i represents the droplet diameter along a particular axis.

Table 2. Average Droplet Diameters and Volumes with Standard Deviations

	100µm Deep Channels with OA	200µm Deep Channels with OA	200µm Deep Channels with LMO
Average Diameter	335 ± 62µm	357 ± 46µm	515 ± 110µm
Average Volume	3.0 ± 1.1µL	6.8 ± 1.6µL	15 ± 5.8µL

There are several possible explanations for the errors in the values of the dimensionless numbers. The first source of error is the fabrication method. Using a mill to cut plastic is not ideal. The polymer chains of the plastic sheet are not easily cut. Rather, they are ripped away from each other and has a very rough finish when observed with the naked eye. The coarse finish must be fixed and the excess plastic from the cutting, or bur, must be removed to allow for good bonding and prevent leaking. This process is done manually and is completely dependent on how steady the hands of the worker is. Couple this coarse finish with the 10µm x,y, and z-direction tolerance of the mill spindle, the relative error can be alarmingly high (±50µm or 25%). The best way to resolve this problem is to explore other fabrication methods. One such method that the author explored, is stereolithography printing (SLA). The absolute tolerance for this platform is very low compared to mechanical methods like milling. One practice piece achieved fluidic channels with a height and width of 50µm ±2um. In this case, the tolerance is dependent on the wavelength of the laser and the vibration of the mirrors directing the laser not the vibration of the cutting tool scraping against the work piece. Due to the small working area of high precision SLA printers, it is not possible to print an entire disk. Microfluidic chips containing the small and sensitive features can be printed and then mounted onto a full disk to address this problem.

Another source of error is the manual loading of the fluids. If oil got into the nozzle, the wetting properties were altered. Even after flushing out the nozzle with water, residue from the

organic phase could have been left behind to affect the flow of the dispersed phase, and, therefore, droplet formation and the dimensionless numbers. A better loading method is needed to prevent this from happening.

Despite the large standard deviation of droplet diameters as a result of unfavorable tolerances in fabrication, it can still be speculated that droplet size was not affected by the volumetric flow rate ratio, the pressure ratio, or the angular velocity. In Figures 10-18, the droplet sizes do not follow a downward trend as φ, $P_{meniscus,c}/P_{meniscus,d}$, and ω increase. This means that the geometry of the FFF is the major factor that determines the droplet size. However, all of these parameters do affect phase flow and whether or not droplets are produced.

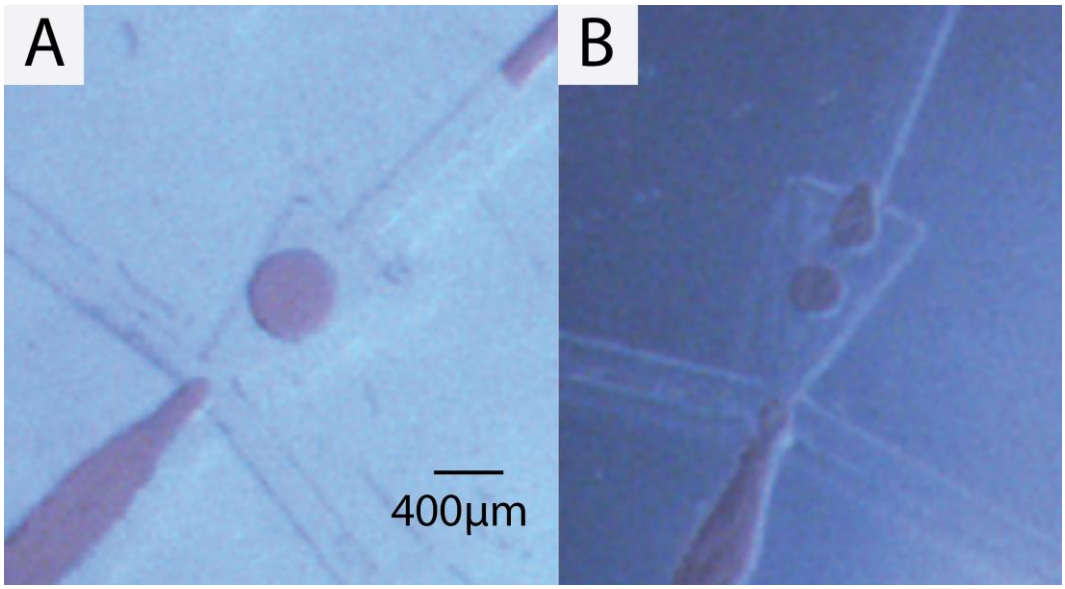

Figure 10. Comparison of droplets produced using different continuous phase solutions. A) Light mineral oil was used as the continuous phase. Droplet sizes were larger on average. This can be attributed to the higher interfacial tension increasing the difficulty in pinching off droplets. B) Oleic acid was used as the continuous phase. Droplet sizes were smaller on average due to the lower interfacial tension of the oleic acid allowing the pinch off of droplets.

In Figures 11-13, the volumetric flow rate ratios are compared to the droplet diameters in each of the fluidic designs. The average droplet diameter did not change when flow rates were varied. This result is not in accordance with the literature, which states the as the continuous phase flow rate increases, the droplets should get smaller until the no flow regime is reached. The same could be said for Figures 14-16 in which the pressure ratios (the pumping forces of each phase), are compared with droplet diameter. Again, the average droplet diameter does not change with varying pressure ratios, confirming the results from the volumetric flow rate ratio comparisons. Lastly, in Figures 17-19, rotational frequency is compared to droplet diameter. As the rotational frequency was increased during the experiments, the average droplet diameter slightly increased, but this has more to do with the constantly decreasing height of the liquid columns. An increasing rotational frequency kept the flow rates and pressures of each phase relatively equal with each other rather than altering droplet size. Future experiments should focus on the previously mentioned problem of precision manufacturing to clear up the discrepancies in this section and find events that more closely resemble those found in the literature.

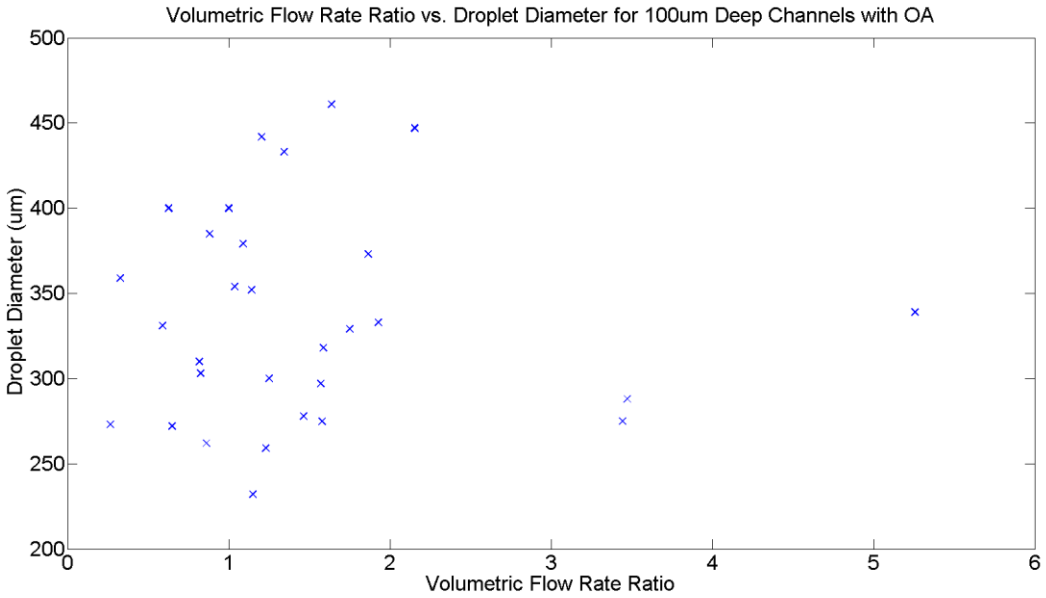

Figure 11. A scatterplot of the volumetric flow rate ratio versus the droplet diameter for the fluidic design with 100µm deep channels using oleic acid as the continuous phase solution. The blue "x" marks are the experimental data gathered.

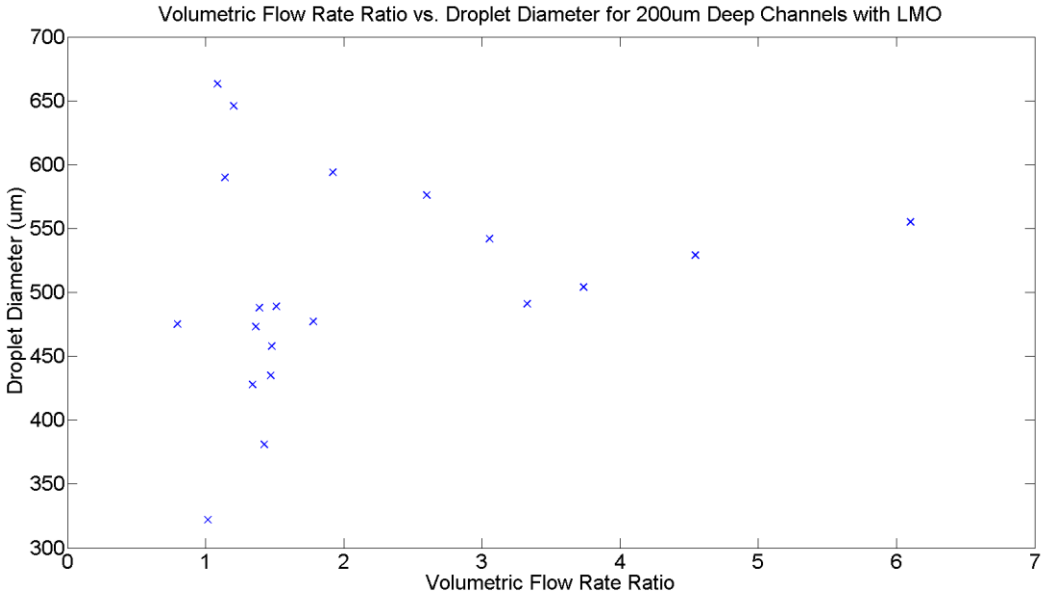

Figure 12. A scatterplot of the volumetric flow rate ratio versus the droplet diameter for the fluidic design with 200µm deep channels using light mineral oil as the continuous phase solution. The blue "x" marks are the experimental data gathered.

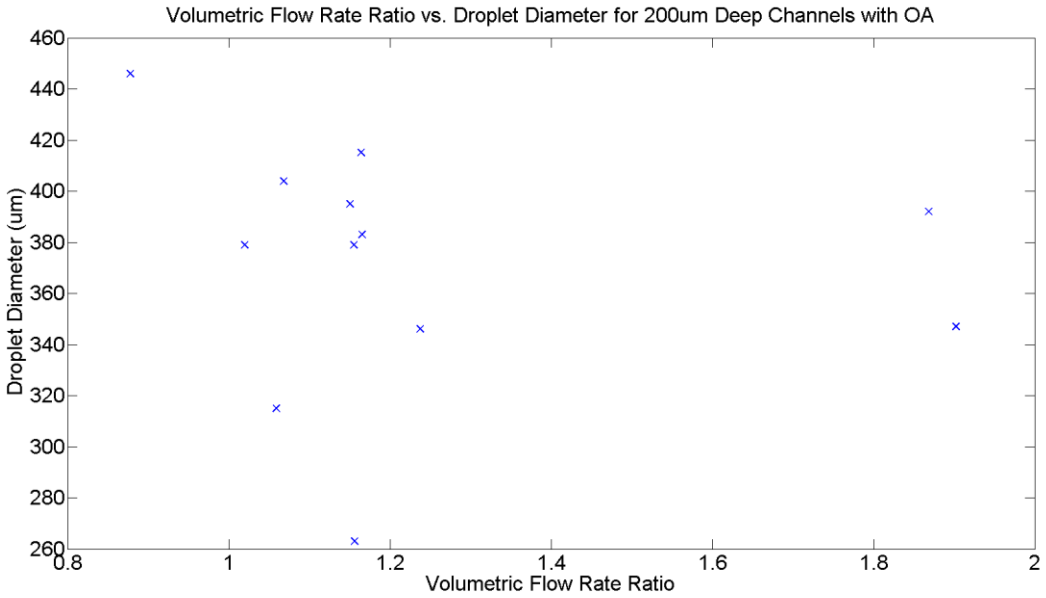

Figure 13. A scatterplot of the volumetric flow rate ratio versus the droplet diameter for the fluidic design with 200µm deep channels using oleic acid as the continuous phase solution. The blue "x" marks are the experimental data gathered.

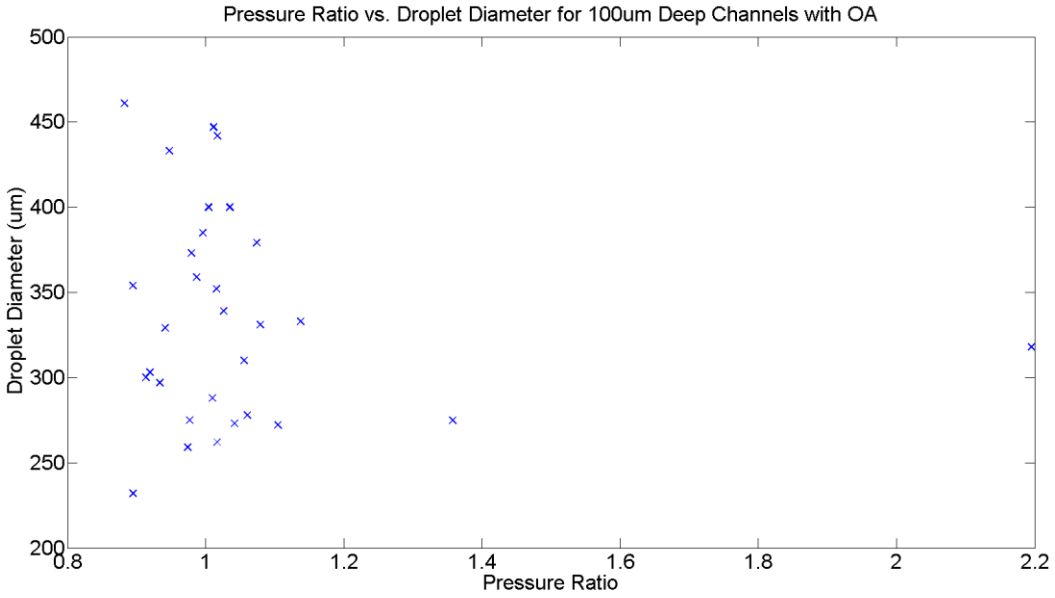

Figure 14. A scatterplot of the pressure ratio versus the droplet diameter for the fluidic design with 100µm deep channels using oleic acid as the continuous phase solution. The blue "x" marks are the experimental data gathered.

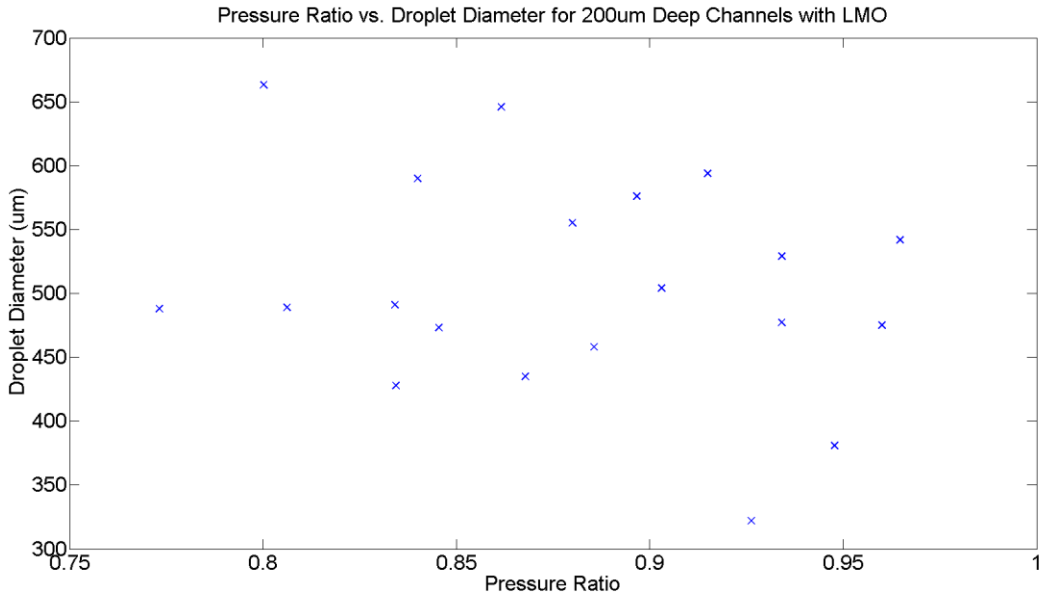

Figure 15. A scatterplot of the pressure ratio versus the droplet diameter for the fluidic design with 200µm deep channels using light mineral oil as the continuous phase solution. The blue "x" marks are the experimental data gathered.

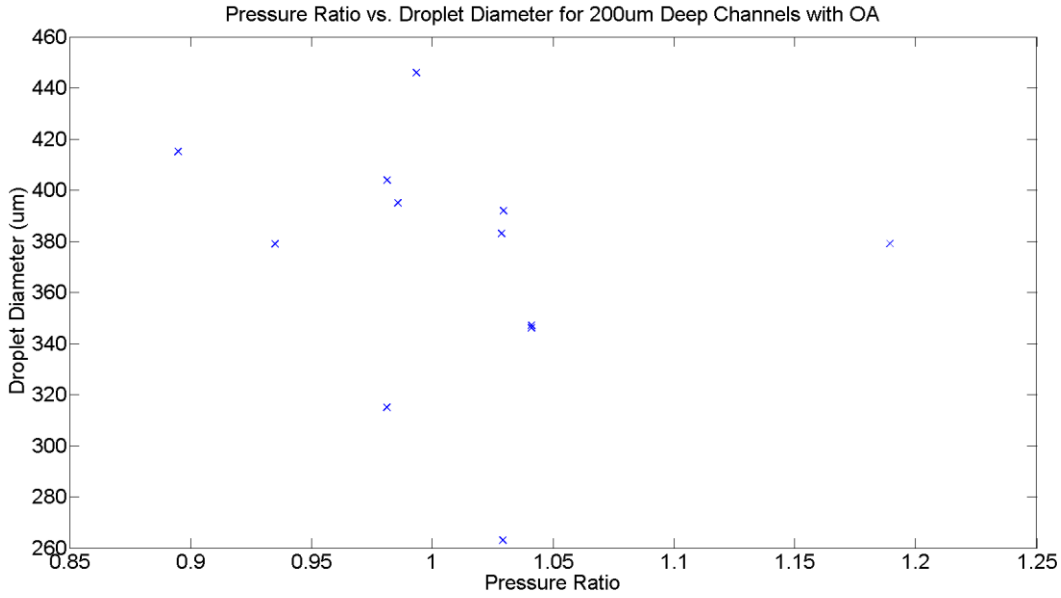

Figure 16. A scatterplot of the pressure ratio versus the droplet diameter for the fluidic design with 200µm deep channels using oleic acid as the continuous phase solution. The blue "x" marks are the experimental data gathered.

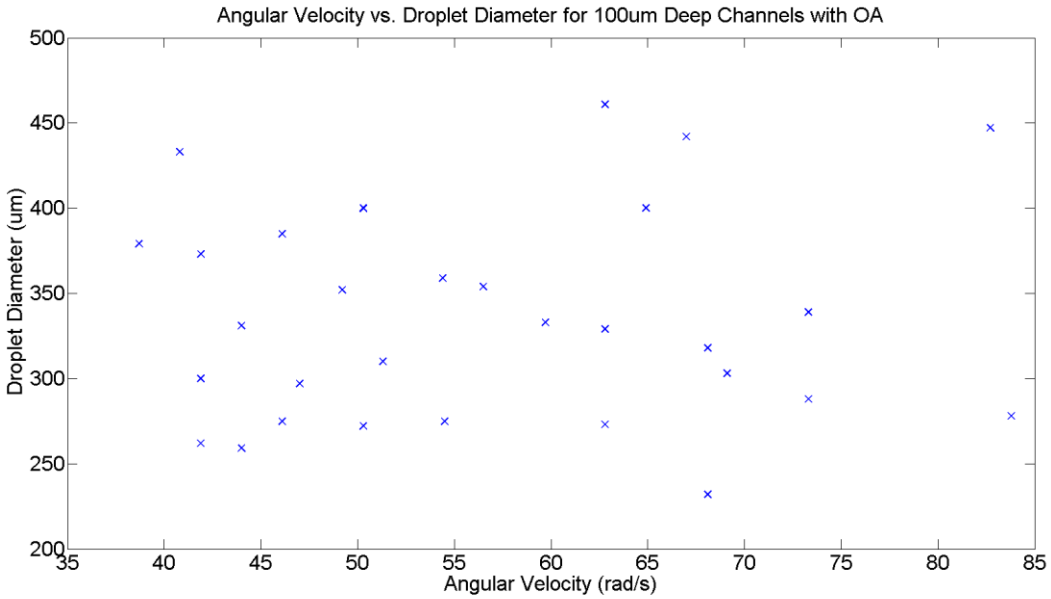

Figure 17. A scatterplot of the angular velocity (rad/s) versus the droplet diameter for the fluidic design with 100µm deep channels using oleic acid as the continuous phase solution. The blue "x" marks are the experimental data gathered.

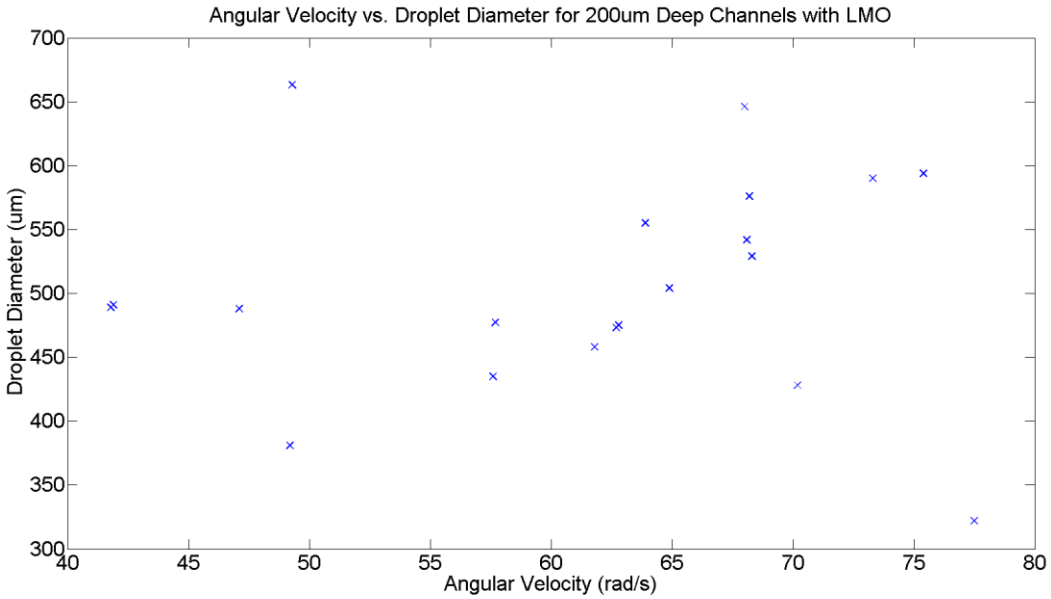

Figure 18. A scatterplot of the pressure ratio versus the droplet diameter for the fluidic design with 200µm deep channels using light mineral oil as the continuous phase solution. The blue "x" marks are the experimental data gathered.

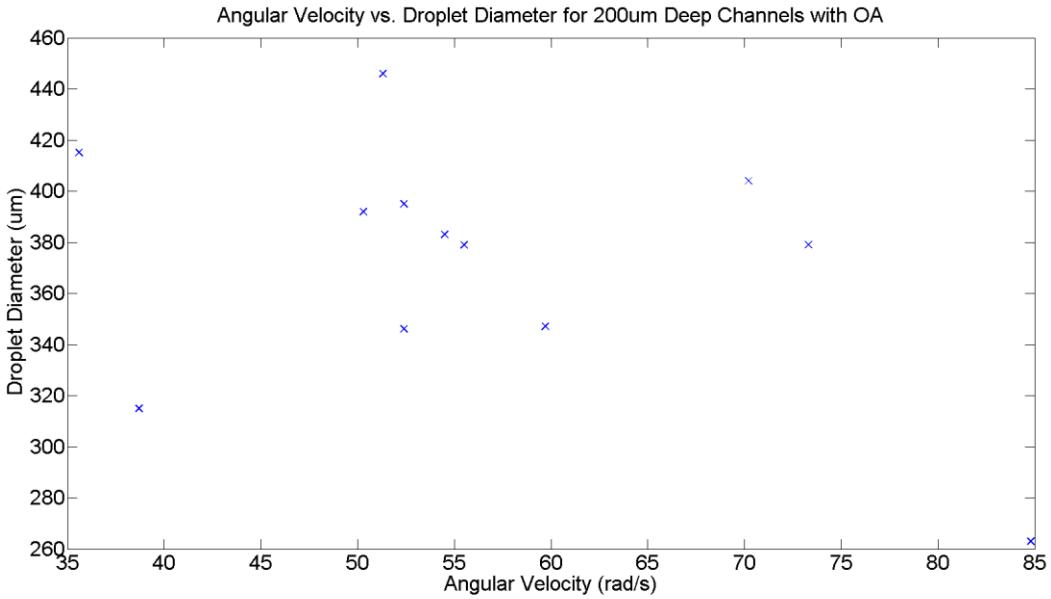

Figure 19. A scatterplot of the angular velocity (rad/s) versus the droplet diameter for the fluidic design with 200µm deep channels using oleic acid as the continuous phase solution. The blue "x" marks are the experimental data gathered.

CHAPTER 4: Conclusion

Droplet microfluidics is an enticing technology that offers significant advantages to the LoD platform. By generating droplets on the scale of nanoliters or smaller, mixing and heating times are reduced due to the shortened diffusion length, reaction times are reduced, tests can be multiplexed, sample volume is decreased, and a high throughput is achieved. The LoD platform complements this technology well with a closed system that can prepare and process raw samples, a variety of valving and other fluid manipulation techniques, a wide range of fluid volumes, a scalable manufacturing capability, and a highly portable format. There are challenges for integrating droplets onto the LoD platform.

Typically the uniform pumping provided by the motor of the centrifugal microfluidic systems is an advantage. Unfortunately, this is not the case for droplet microfluidics as it is not possible to change the pressure gradients and flow rate of each phase independently during an experiment. If the angular velocity is changed, all of the fluidics on the disk are altered accordingly. Thus, all of the pressure gradients and flow rates must be determined during the design phase.

Another challenge that was briefly touch on is the continuous change of the fluid column heights. As the liquids are drained from the chambers, the heights of their fluid column change. This constantly decreases the pressure gradients to a point where there is not enough fluid flow for droplet formation. A model for droplet production would aid in developing a spin profile that would automatically increase the rotations-per-minute (RPM) in coordination with the lowering fluid column heights.

This work has taken steps toward developing a model that can predict droplet formation and size. A thorough literature search has provided guidelines to follow to produce droplets

based on dimensionless numbers (Ca, We, and Bo numbers) and the ratio of the dispersed phase and continuous phase volumetric flow rates. The capillary number is the ratio of viscous forces versus surface tension acting across the interface between the two immiscible phases. The Weber number represents the ratio of inertial forces to surface tension forces between fluids. The Bo number is defined as the ratio between gravitational forces and surface tension forces. Droplet generation occurs in the "dripping regime" and is generally defined by the critical values of these dimensionless numbers: $Ca_{crit} \sim 0.1$, $We_{crit} = 1$, and $Bo_{crit} = 1$. If the calculated values of both the Ca and We numbers fall below their critical values, and the calculated value of the Bo number was above the critical values, the system should be in the "dripping regime."

Another parameter that determines droplet formation is the ratio of the continuous and dispersed volumetric flow rates, φ. The "dripping regime" is near $\varphi \geq 1$. If the volumetric flow rates follow this parameter, droplets are produce. The co-flow or jetting regime is when $\varphi < 1$. The two phases will flow side-by-side since the continuous phase is not flowing fast enough to overcome the surface tension forces and pinch off droplets from the water stream. The "no flow regime" is when $\varphi >> 1$. The water column is not allowed to flow out of the nozzle due to the weak hydrodynamic force. With these conditions in mind, an equation describing the radial position of each fluid column and their heights was derived. In accordance with Equation (15), the fluidic features of the disk were designed. The disks were manufactured out of PC sheets with channel depths of 100µm and 200 µm and bonded together using PSA.

A variety of organic solutions were tried, but OA and LMO were chosen as the continuous phase solutions as they had the best compatibility with the microfluidic disks and have been studied extensively, providing a solid information base for calculating the dimensionless numbers. OA and LMO are also currently some of the most common solutions

used for droplet production. The water-oil systems were loaded into the disks and tested on a custom spin stand testing platform equipped with a servo motor to rotate the CDs and high speed camera to capture the events happening in the channels and chambers. The flow rates, angular velocity, and droplet diameters were recorded. The fluid column heights were also recorded and then used to calculate $P_{meniscus}$ for each phase. The ratio between P_{oil} and P_{water} was useful in finding the conditions need to produce droplets. Previous literature regarding droplets being generated at $\varphi \geq 1$ and $P_{oil}/P_{water} \geq 1$ were confirmed as droplets emulsions were successfully replicated. The angular velocities, volumetric flow rate ratios, and pressure ratios were compared to droplet size. There was no correlation between droplet size and any change in these parameters, implying that the geometry of the channels has the most influence over droplet size.

Analyzing the dimensionless numbers was not as successful. Once the experimental values of the dimensionless numbers were calculated, We number values followed the literature in that they were below the critical value, allowing droplet formation. The Bo numbers were above the critical value, but seemed off from the literature. The calculated Ca numbers were above their critical value, indicating that there should be no droplet formation, despite the successful trials. These strange results can be rectified by changing the fabrication process from milling plastic to a more precise prototyping machine like a SLA printer. A new loading method is also needed to prevent oil from wetting the nozzle and altering the flow of the dispersed phase.

Future research for droplets on the LoD platform should focus on developing a predictive model for the formation of droplets. While this work has taken steps towards achieving this goal, better characterization using dimensionless numbers is a key component to understand droplet formation and building such a model.

Future experiments should focus on utilizing better precision manufacturing technologies, such as SLA printing to address the tolerance problems in fabrication. The coarse finish from the plastic being milled must be removed to allow for good bonding and prevent leaking. This process is done manually, leading to significant and inconsistent errors. In combination with this process, the spindle of the CNC mill used had a 10µm x,y, and z-direction tolerance, the relative error can be exceptionally high. The best way to resolve this problem is to explore other fabrication methods. Once a more precise fabrication technique is found, it can be utilized to elaborate on the contribution of dimensionless numbers to droplet formation on CDs.

Another direction for research should be applications and achieving a higher throughput for droplets on CDs. Because of the versatility of droplet technology, a wide range of applications is available for exploration. Digital PCR, cell encapsulation, and droplets as microreaction chambers are all viable options that could be integrated onto the LoD platform. For these applications, it is necessary to study the effects that surfactants have on droplet formation. Characterization by dimensionless numbers would contribute substantially in building a model that incorporates surfactants into the surface tension force balance.

Finally, increasing the throughput of the LoD platform to be more comparable to the LoC devices is another area of research that should be investigated. The real estate on microfluidic CDs is limited, but the MIMEMS group in Malaysia has begun to look at their fluidics in three dimensions rather than two. It is possible to have separate channels above and below each other depending on the organization of the channels in the layers of the disk.[48] This opens up the LoD platform to even more complicated laboratory and diagnostic protocols.

REFERENCES

(1) Shim, J. U.; Ranasinghe, R. T.; Smith, C. a.; Ibrahim, S. M.; Hollfelder, F.; Huck, W. T. S.; Klenerman, D.; Abell, C. *ACS Nano* **2013**, *7*, 5955–5964.

(2) Milas, P.; Rahmanseresht, S.; Ramos, K. P.; Gamari, B. D.; Goldner, L. S. **2013**.

(3) Tan, Y.-C.; Collins, J.; Lee, A. P. In *MircoTAS*; 2003.

(4) Teh, S.-Y.; Lin, R.; Hung, L.-H.; Lee, A. P. *Lab Chip* **2008**, *8*, 198–220.

(5) Guo, M. T.; Rotem, A.; Heyman, J. a.; Weitz, D. a. *Lab Chip* **2012**, *12*, 2146.

(6) Hatch, A. C.; Fisher, J. S.; Tovar, A. R.; Hsieh, A. T.; Lin, R.; Pentoney, S. L.; Yang, D. L.; Lee, A. P. *Lab Chip* **2011**, *11*, 3838–3845.

(7) RainDrop Digital PCR System http://raindancetech.com/digital-pcr-tech/raindrop-digital-pcr-system/ (accessed Feb 23, 2015).

(8) Hindson, C. M.; Chevillet, J. R.; Briggs, H. a; Gallichotte, E. N.; Ruf, I. K.; Hindson, B. J.; Vessella, R. L.; Tewari, M. *Nat. Methods* **2013**, *10*, 1003–1005.

(9) Gursoy, R. N.; Benita, S. *Biomed. Pharmacother.* **2004**, *58*, 173–182.

(10) Fisher, J. S.; Lee, A. P. In *MicroTAS*; 2004.

(11) Tan, Y.-C.; Hettiarachchi, K.; Siu, M.; Pan, Y.-R.; Lee, A. P. *J. Am. Chem. Soc.* **2006**, *128*, 5656–5658.

(12) Clausell-Tormos, J.; Lieber, D.; Baret, J. C.; El-Harrak, A.; Miller, O. J.; Frenz, L.; Blouwolff, J.; Humphry, K. J.; Köster, S.; Duan, H.; Holtze, C.; Weitz, D. a.; Griffiths, A. D.; Merten, C. a. *Chem. Biol.* **2008**, *15*, 427–437.

(13) Freitas, S.; Hielscher, G.; Merkle, H. P.; Gander, B. *Ultrason. Sonochem.* **2006**, *13*, 76–85.

(14) Noireaux, V.; Libchaber, A. *Proc. Natl. Acad. Sci. U. S. A.* **2004**, *101*, 17669–17674.

(15) Chen, H.; Zhao, Y.; Li, J.; Guo, M.; Wan, J.; Weitz, D. a; Stone, H. a. *Lab Chip* **2011**, *11*, 2312–2315.

(16) Madou, M.; Zoval, J.; Jia, G.; Kido, H.; Kim, J.; Kim, N. *Annu. Rev. Biomed. Eng.* **2006**, *8*, 601–628.

(17) Anderson, N. G. *Fresenius' Zeitschrift f*  *r Anal. Chemie* **1972**, *261*, 257–271.

(18) Gorkin, R.; Park, J.; Siegrist, J.; Amasia, M.; Lee, B. S.; Park, J.-M.; Kim, J.; Kim, H.; Madou, M.; Cho, Y.-K. *Lab Chip* **2010**, *10*, 1758–1773.

(19) Madou, M. J. *Fundamentals of microfabrication: the science of miniturization*, 3rd ed.; CRC Press, 2011; p 1992.

(20) Kido, H.; Micic, M.; Smith, D.; Zoval, J.; Norton, J.; Madou, M. *Colloids Surfaces B Biointerfaces* **2007**, *58*, 44–51.

(21) Haeberle, S.; Brenner, T.; Zengerle, R.; Ducrée, J. *Lab Chip* **2006**, *6*, 776–781.

(22) Brenner, T.; Glatzel, T.; Zengerle, R.; Ducre, J.; Koehler-allee, G. *Int. Conf. miniaturized Chem. Biochem. Anal. Syst.* **2003**, 903–906.

(23) Amasia, M.; Cozzens, M.; Madou, M. J. *Sensors Actuators, B Chem.* **2012**, *161*, 1191–1197.

(24) Abi-Samra, K.; Hanson, R.; Madou, M.; Gorkin, R. a. *Lab Chip* **2011**, *11*, 723–726.

(25) Garcia-Cordero, J. L.; Kurzbuch, D.; Benito-Lopez, F.; Diamond, D.; Lee, L. P.; Ricco, A. J. *Lab Chip* **2010**, *10*, 2680–2687.

(26) Noroozi, Z.; Kido, H.; Madou, M. J. *J. Electrochem. Soc.* **2011**, *158*, P130.

(27) Abi-Samra, K.; Clime, L.; Kong, L.; Gorkin, R.; Kim, T. H.; Cho, Y. K.; Madou, M. *Microfluid. Nanofluidics* **2011**, *11*, 643–652.

(28) Amasia, M.; Madou, M. *Bioanalysis* **2010**, *2*, 1701–1710.

(29) Berthier, J.; Silberzan, P. *Microfluidics for Biotechnology*; Artech House, 2010; p 483.

(30) Haeberle, S.; Zengerle, R.; Ducrée, J. *Microfluid. Nanofluidics* **2006**, *3*, 65–75.

(31) Garstecki, P.; Fuerstman, M. J.; Stone, H. a; Whitesides, G. M. *Lab Chip* **2006**, *6*, 437–446.

(32) Gupta, A.; Murshed, S. M. S.; Kumar, R. *Appl. Phys. Lett.* **2009**, *94*, 94–97.

(33) Cozzens, M. A. Droplet Generation on a Centrifugal Disc: Novel Applications and Numerical Characterization Studies, University of California, Irvine, 2011, pp 1–51.

(34) Tan, Y.-C.; Cristini, V.; Lee, A. P. *Sensors Actuators B Chem.* **2006**, *114*, 350–356.

(35) Kamogawa, K.; Okudaira, G.; Matsumoto, M.; Sakai, T.; Sakai, H.; Abe, M. *Langmuir* **2004**, *20*, 2043–2047.

(36) Opawale, F. O.; Burgess, D. J. *J. Colloid Interface Sci.* **1998**, *197*, 142–150.

(37) Anna, S. L.; Bontoux, N.; Stone, H. a. *Appl. Phys. Lett.* **2003**, *82*, 364–366.

(38) Christopher, G. F.; Anna, S. L. *J. Phys. D. Appl. Phys.* **2007**, *40*, R319–R336.

(39) Lee, W.; Walker, L. M.; Anna, S. L. *Phys. Fluids* **2009**, *21*.

(40) Chakraborty, D.; Chakraborty, S. *Appl. Phys. Lett.* **2010**, *97*, 234103.

(41) Lee, J.; Moon, H.; Fowler, J.; Schoellhammer, T.; Kim, C. J. *Sensors Actuators, A Phys.* **2002**, *95*, 259–268.

(42) Shen, H. H.; Fan, S. K.; Kim, C. J.; Yao, D. J. *Microfluid. Nanofluidics* **2014**, *16*, 965–987.

(43) Subedi, D.; Tyata, R.; Rimal, D. *... Univ. J. Sci. Eng. ...* **2009**, *5*, 37–41.

(44) Ma, Y.; Cao, X.; Feng, X.; Ma, Y.; Zou, H. *Polymer (Guildf).* **2007**, *48*, 7455–7460.

(45) Koos, E.; Johannsmeier, J.; Schwebler, L.; Willenbacher, N. *Soft Matter* **2012**, *8*, 6620.

(46) Shively, M. L. *Pharm. Res. 10*, 1153–1156.

(47) Opawale, F.; Burgess, D. *J. Colloid Interface Sci.* **1998**, *197*, 142–150.

(48) Thio, T. H. G.; Ibrahim, F.; Al-Faqheri, W.; Moebius, J.; Khalid, N. S.; Soin, N.; Kahar, M. K. B. A.; Madou, M. *Lab Chip* **2013**.

APPENDIX A: Symbols

In order of appearance:

Q_{water}	volumetric flow rate of the water or aqueous phase.
Q_{oil}	volumetric flow rate of the oil or organic phase.
Ca	capillary number used to characterize the ratio of viscous forces versus surface tension acting across the interface between the two immiscible phases.
μ_c	dynamic viscosity of the continuous phase.
γ	interfacial tension between the continuous and dispersed phases.
We	Weber number used to characterize the ratio of inertial forces to surface tension forces between fluids.
ρ_i	density of a specific phase or liquid.
v_d	velocity of the dispersed phase in calculating the Weber number in Equation (2).
l	characteristic geometry of a fluidic channel.
σ	surface tension of the dispersed phase.
φ	volumetric flow rate ratio Q_c/Q_d.
Bo	Bond number used to characterize the relationship between gravitational forces and surface tension forces.
ω	angular velocity of the disk.
z	characteristic geometry for the angular velocity.
Q_i	volumetric flow rate of a specific phase.
$\bar{r}$	average fluid column height.
Δr	difference in radial positions of the menisci of a single fluid.
R	fluidic resistance of the channels.

L_i	length of the observed channel.
$A_{cs,i}$	cross-sectional area of the channel of a certain phase
$D_{h,i}$	hydraulic diameter of the channel ($4A_{cs,i}/P$).
P	wetted perimeter of the channel.
$P_{meniscus}$	hydrodynamic force at any radial position on the CD.
P_γ	Laplace pressure.
θ_c	equilibrium contact angle.